Combustion Theory and Modelling
Vol. 00, No. 00, May 2014, 1–25

RESEARCH ARTICLE

RANS predictions of flame lift-off: comparison of a reactor and a flamelet combustion model to the well stirred approach

Anne Kösters [a*], Anders Karlsson [ab], Michael Oevermann [a], Gianluca D'Errico[c] & Tommaso Lucchini [c]

[a] *Department of Applied Mechanics, Chalmers University of Technology, Sweden*
[b] *Volvo Group Advanced Technology and Research, Sweden*
[c] *Dipartimento di Energi, Politecnico di Milano, Italy*

(*vX.X released May 2014*)

The flame stabilization process in turbulent non-premixed flames is not fully understood and several models have been developed to describe the turbulence-chemistry interaction. This work compares the performance of the multiple representative interactive flamelet (mRIF) model, the Volume Reactor Fraction Model (VRFM), and the well stirred reactor (WS) model in describing such flames. The predicted ignition delay and flame lift-off length of n-heptane sprays are compared to experimental results published within the Engine Combustion Network (ECN). All of the models predict the trend of ignition delay reasonably well. At a low gas pressure (42 bar) the ignition delay is overpredicted compared to the experimental data, but the difference between the models is not significant. However, the predicted lift-off lengths differ. At high pressure (87 bar) the difference between the models is small. All models slightly underpredict the lift-off length compared to the experimental data. At low gas pressure (42 bar) the mRIF model gives best results. The VRFM and the WS model predict excessively short lift-off lengths, but the VRFM gives better results than the WS model. The flame structures of the models are also compared. The WS model and the VRFM yield a well defined flame stabilization point whereas the mRIF model does not. The flame of the mRIF model is more diffuse and the model is not able to predict flame propagation. All models were able to predict the experimental trends in lift-off and ignition delay, but certain differences between them are demonstrated.

Keywords: spray, combustion, turbulence, flame lift-off, RIF

Index to information contained in this guide

*Anne Kösters. Email: anne.kosters@chalmers.se

ISSN: 1364-7830 print/ISSN 1741-3559 online

DOI: 10.1080/13647830.YYYY.xxxxxx
http://www.tandfonline.com

1. Introduction

1.1 Background

Diesel combustion is a very complex process. Liquid Diesel fuel is injected directly into the combustion chamber where the liquid core of the spray breaks up into droplets which then evaporate. The fuel vapor mixes with the air and ignites. The combustion is mixing controlled, meaning that the fuel and air must mix before combustion; in cases involving fast chemistry, the rate of mixing controls the reaction rate. A detailed description of all of these processes is therefore required to accurately model Diesel combustion. Many combustion models are based on scale separation. The chemical time-scale is assumed to be much faster than the turbulent time-scale (Damköhler number $Da \gg 1$), which determines the reaction rate. The assumption of scale separation requires the reaction layer to be thinner than the smallest turbulent scales, which are characterized by the Kolmogorov length scale. In cases where this is true, the reaction layer is not affected by turbulence. Well known approaches for modeling non-premixed turbulent combustion include the flamelet concept [1] and the Eddy Break-Up (EBU) model [2]. Many works have discussed these different models and their advantages and disadvantages, but most of these studies focused on a single model implemented in a certain CFD code. This makes it rather difficult to meaningfully compare the merits of the different approaches. In addition, the results of CFD simulations depend on the discretization schemes that are used and the mesh resolution. We therefore sought to compare the performance of the different models side-by-side using an identical computational configuration in each case, with minimal differences between the numerical set-ups used for each model.
To this end, we compared the Volume Reactor Fraction Model (VRFM) [3], the multiple representative interactive flamelet (mRIF) model [4], and the well-stirred reactor (WS) model using the open-source software package OpenFOAM®. The VRFM describes the turbulence-chemistry interaction with a partially stirred reactor (PaSR) approach [5]. The PaSR approach is based on the Eddy Dissipation Concept (EDC) of Magnussen [6], which is a more extensively developed version of the Eddy Dissipation Combustion Model [7]. The EDC is a well-known method for describing turbulence-chemistry interactions in a way that includes sub-grid scale interactions and enables the simulation of complex chemistry mechanisms. In both models, a reactor volume $V_{reactor}$ is defined that is smaller than the cell volume and controls the reaction rate. The main difference between the VRFM and the EDC is the definition of the reactor volume. The VRFM has previously been used to investigate the effects of the EGR level on the flame lift-off length [3]. In both models, chemical conversion takes place in a perfectly stirred reactor, i.e., they do not consider any (underlying laminar) flame structure. Other studies using the EDC are published in references [8], [9], [10] and [11]. The WS model uses a simpler approach in which the entire CFD cell is assumed to be well-mixed. This model has been used by authors such as [12]. An alternative approach to modeling turbulent non-premixed combustion is based on the flamelet concept. A flamelet is a thin reactive diffusive layer embedded within a turbulent flow field. In cases involving large Damköhler numbers, the chemical time scales are shorter than the turbulent time scales. This makes it possible to model the local turbulent non-premixed flame structure as an ensemble of one dimensional parameterized laminar flames within a turbulent flow field. The flame surface is defined as the isosurface of a non-reacting scalar such as the mixture fraction Z for non-premixed turbulent combustion under stoichiometric conditions. According to this definition, each species' mass fraction and temperature can be defined

based on the mixture fraction Z, the time t, and the scalar dissipation rate. The unsteady flamelet equations were derived by Peters in 1984 [1]. The coupling of the CFD solution with an unsteady flamelet is given by the representative interactive flamelet (RIF) concept [4]. This method uses a presumed pdf to transform mass fractions defined in mixture fraction space back to CFD space. As a result, instead of solving transport equations for all species mass fractions in CFD space, only the mixture fraction and its variance need to be solved to determine the presumed pdf. The big advantage of this approach is that the chemistry is decoupled from the flow field, which significantly reduces the computational time.

Singh et al. [13] compared the performance of the RIF model, the Characteristic Time Combustion (CTC) model, and the direct chemistry approach (the well-stirred model) in modeling non-premixed turbulent combustion using the KIVA software. In general, all three models predicted the cylinder pressure and heat release with reasonable accuracy. However, the RIF model was more sensitive to the chemistry, which affected its prediction of the ignition delay. The RIF models predictions of NOx emissions were slightly sensitive to the number of flamelets, while those of the CTC model were more sensitive to the model constants. The CTC model calculates the equilibrium concentration of all species and the corresponding laminar and turbulent characteristic times, which are used to define the rate of change of the species [14]. Each model provided a somewhat different predicted flame structure. The study reported herein was conducted to compare three different approaches to combustion modeling, namely the VRFM, RIF and WS models, with all three models being implemented in the same software package. Each model was used to simulate the combustion of an n-heptane spray and the results obtained were compared to experimental data collected within the Engine Combustion Network (ECN) [15]. Today, the ECN is a well known data-base and its experimental data have been used for validation purposes in many other works. A good overview of different publications dealing with modeling of the ECN cases is given by [16]. This work focuses on comparing the predicted flame structure, ignition delay and lift-off length obtained with different combustion models. All of the combustion models are used to simulate sprays with identical set-ups, enabling their direct comparison.

1.2 Turbulent Jet Diffusion Flame

In 1997 Dec presented a conceptual model of DI Diesel Combustion [17] that was based on experimental data obtained using laser-sheet imaging. The model describes the development of a typical Diesel jet diffusion flame in terms of a sequence of distinct events that occur at different times after the start of injection. One key finding of his study is that after the premixed fuel is burned, the flame is exclusively mixing controlled. Dec concluded that soot production is high in the leading portion of the burning jet but low just downstream of the vapor fuel area. The diffusion flame appears at the stoichiometric edge of the jet. Interestingly, it was also proposed that there is a "standing premixed flame throughout the mixing-controlled burn". **In 1996 this was already shown with a modeling approach by Chomiak and Karlsson [5].** This implies that the reactants in the diffusion flame are the products of the fuel-rich premixed combustion process and air. Prior to this, the general assumption was that the mixing reactants in a diffusion flame are fuel and air. In addition, before Dec published his conceptual model, the premixed combustion in a DI Diesel flame was assumed to occur under stoichiometric conditions and the depth of penetration of the liquid phase was as-

sumed to be larger, with combustion occurring only in the peripheral region of the jet. Soot production was therefore assumed to occur only in the edging region of the jet with the diffusion flame, as discussed by [18], [19] and [20]. In 2005 Pickett et al. [21] published their analysis of the effects of ignition processes on flame stabilization in Diesel jet diffusion flames. They used chemiluminescence imaging to analyze the ignition and combustion regions of the fuel jet and conducted pressure measurements to determine the ignition delay time. Several fuels with different cetane-numbers were considered. Their results indicated that "a one-to-one correlation between lift-off length and ignition delay does not always exist." In addition, they found that the lift-off length does not correlate with flame propagation; instead, it correlates with the location of the cool-flame base. It was suggested that this may occur because the time required for the transition from first-stage ignition to second-stage high-temperature combustion differs between fuels. To summarize, the physics of the flame stabilization process in turbulent jet flame are still not fully understood. Existing models for describing the combustion process in diesel spray flames are, to some extent, based on theoretical investigations. A better understanding based on experimental results is thus needed to enable the further development of the mathematical models that are used in CFD simulations. To this end, we investigated the performance of the modeling approaches discussed in the preceding sections and compared their predictions to existing experimental results.

2. Modeling Approach

2.1 Mixture Fraction Z

The mixture fraction $\widetilde{Z}$ defines the local ratio of fuel mass per air mass and is an indicator of the degree of mixing. The transport equations for the mixture fraction $\widetilde{Z}$ and its variance $\widetilde{Z^{"2}}$ are given by equations (1) and (2).

$$\frac{\partial(\overline{\rho}\widetilde{Z})}{\partial t} + \nabla\cdot(\overline{\rho}\widetilde{\mathbf{u}}\widetilde{Z}) = \nabla\left[\frac{\mu_t}{Sc_t}\nabla\widetilde{Z}\right] + \dot{S}_{evap}, \tag{1}$$

$$\begin{aligned}\frac{\partial(\overline{\rho}\widetilde{Z^{"2}})}{\partial t} + \nabla\cdot(\overline{\rho}\widetilde{\mathbf{u}}\widetilde{Z^{"2}}) = \nabla\left[\frac{\mu_t}{Sc_{t,Z^{"2}}}\nabla\widetilde{Z^{"2}}\right] + 2\frac{\mu_t}{Sc_t}(\nabla\widetilde{Z})^2 - \overline{\rho}\widetilde{\chi}_Z \\ +2(1-\widetilde{Z})\overline{\rho}\widetilde{Z^{"2}\dot{S}} - \overline{\rho}\widetilde{Z^{"2}\dot{S}},\end{aligned} \tag{2}$$

where Sc_t is the turbulent Schmidt number, u the velocity, ρ the density and μ_t the turbulent viscosity. The scalar dissipation rate $\widetilde{\chi}$ is defined by

$$\widetilde{\chi} = 2D\widetilde{(\nabla Z^{"2})}^2. \tag{3}$$

where D is the diffusion coefficient. The source terms due to evaporation (last two terms in equation (2)) are closed with the approach presented by Réveillon and Vervisch [22] and Hasse subsequently expanded the source terms around their

mean values and introduced the method into the RIF model [23]. The final expression for variance of the mixture fraction $\widetilde{Z''^2}$ is thus given by equation (4).

$$\begin{aligned}\frac{\partial(\overline{\rho}\widetilde{Z''^2})}{\partial t} + \nabla\cdot(\overline{\rho}\widetilde{\mathbf{u}}\widetilde{Z''^2}) = \nabla\left[\frac{\mu_t}{Sc_{t,Z''^2}}\nabla\widetilde{Z''^2}\right] + 2\frac{\mu_t}{Sc_{t,Z''^2}}(\nabla\widetilde{Z})^2 - \\ \frac{3c_\chi C\tau}{1-e^{-3C_\tau}}\frac{\widetilde{\varepsilon}}{\widetilde{k}}\widetilde{Z''^2} + \alpha_{B_Y}\left(2\left[\xi\widetilde{Z}^{\xi-1} - (\xi+1)\widetilde{Z}^{\xi}\right]\widetilde{Z''^2}\right),\end{aligned} \tag{4}$$

with $\tau = \frac{\widetilde{k}}{\widetilde{\varepsilon}}$ and C is calculated via

$$C = \alpha_{B_Y}\left[\xi\widetilde{Z}^{\xi-1} - (\xi+1)\widetilde{Z}^{\xi}\right]. \tag{5}$$

Réveillon and Vervisch suggest $\xi = 2$ and α_{B_Y} can be extracted from

$$\overline{\rho}\widetilde{\dot{S}} = \overline{\rho}\int_Z \alpha_{B_Y}(Z^*)^{\xi}\widetilde{P}(Z^*)dZ^*. \tag{6}$$

2.2 WS model

The approach of the WS model does not include any sub-grid scale effects. The source term of the chemistry, $\dot{\omega}_i$, is thus included in the transport equation of the species, Y_i, see equation (7).

$$\frac{\partial}{\partial t}\overline{\rho}\widetilde{Y_i} + \nabla(\overline{\rho}\widetilde{\mathbf{u}}\widetilde{Y_i}) = -\triangle\mu_{eff}\widetilde{Y_i} + \dot{\omega}_i + \dot{S}_{i,evap} \tag{7}$$

where μ_{eff} is the effective viscosity. This is the simplest way of including the chemistry source term, but it is computationally expensive because it requires the solution of a transport equation for each individual species involved in the chemical mechanism.

2.3 VRFM

The VRFM was developed to describe the sub-grid scale effects of turbulence and chemistry during combustion. To this end, it is assumed that reactions may only occur within a reactor whose volume is smaller than or equal to that of the computational cell ($V_{reactor} \leq V_{cell}$) and is defined as a fraction of the cell volume:

$$\kappa = \frac{V_{reactor}}{V_{cell}} = \left(1 - \frac{\widetilde{Z''^2}}{\widetilde{Z}(1-\widetilde{Z})}\right)\left(1 - \frac{\widetilde{c''^2}}{\widetilde{c}(1-\widetilde{c})}\right). \tag{8}$$

Reactions are only allowed to occur in the reactor. The reactor volume is defined in terms of the variance of the mixture fraction, $\widetilde{Z}$, and the chemical progress, $\widetilde{c}$. The terms $\widetilde{Z}(1-\widetilde{Z})$ and $\widetilde{c}(1-\widetilde{c})$ define the maximum variance of the mixture fraction and chemical progress. That means, in case of strong variance of either

mixture fraction ($\widetilde{Z''^2} \approx \widetilde{Z}(1-\widetilde{Z})$) or chemical progress ($\widetilde{c''^2} \approx \widetilde{c}(1-\widetilde{c})$), the reactor volume fraction will be much smaller than 1. A high degree of variation in the mixture fraction is indicative of poor mixing, while strong variation in the chemical progress is observed during the ignition phase and other processes when there are steep gradients in chemical progress within the cell. If both variances are low, meaning that the species in the cell are well mixed and the chemical reactions are homogeneously developed, the reactor volume will be similar or equal to the cell volume ($\kappa \approx 1$). This definition solves the problem of identifying representative time-scales for mixing and for chemical reactions. In a diffusion flame the chemical reactions are controlled by the mixing rate. This means that not all species will be consumed at $\widetilde{Z}_{st}$. According to Burke and Schumann [24], the concentrations of each species can be defined based on the mixture fraction. Before burning, fuel and oxygen are linearly distributed throughout the mixture fraction, with opposite gradients. During burning, the level of both fuel and oxygen will be zero for a stoichiometric mixture fraction because fuel and oxygen are both entirely consumed as shown in Figure 1. The chemical progress is therefore defined in terms of the remaining mass fraction of fuel in lean mixtures ($\widetilde{Z} < \widetilde{Z}_{st}$) and the remaining mass fraction of oxygen in rich mixtures ($\widetilde{Z} > \widetilde{Z}_{st}$), as shown in equation (9).

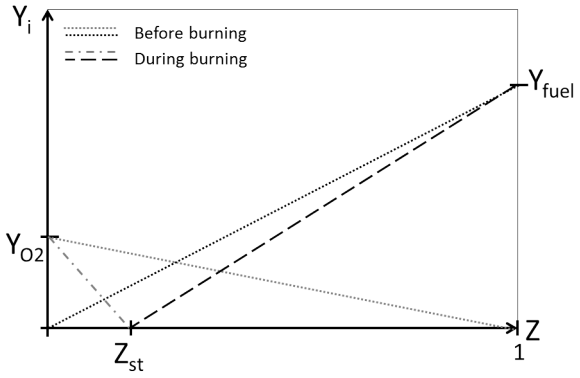

Figure 1. Correlation between oxygen and fuel mass fraction (adapted from [24])

$$\widetilde{c} = \begin{cases} 1 - \dfrac{\widetilde{Y}_{fuel}}{\widetilde{Z}} & \text{if} \quad \widetilde{Z} \leq \widetilde{Z}_{st}, \\ 1 - \dfrac{\widetilde{Y}_{\mathrm{O}_2}}{(\widetilde{Y}_{\mathrm{O}_2})_{air}(1-\widetilde{Z})} & \text{if} \quad \widetilde{Z} > \widetilde{Z}_{st}. \end{cases} \tag{9}$$

$(\widetilde{Y}_{\mathrm{O}_2})_{air}$ is the initial mass fraction of oxygen in the air. The transport equation for the variance of the chemical progress, $\widetilde{c''^2}$, is given by equation (10) in analogy with the equation for the variance of the mixture fraction (equation (2)):

$$\frac{\partial(\overline{\rho}\widetilde{c''^2})}{\partial t} + \nabla\cdot(\overline{\rho}\widetilde{\mathbf{u}}\widetilde{c''^2}) = \nabla\left[\frac{\mu_t}{Sc}\nabla\widetilde{c''^2}\right] + 2\frac{\mu_t}{Sc}(\nabla\widetilde{c})^2 - \overline{\rho}\widetilde{\chi}_C + 2\widetilde{c''\dot{\omega}_i^R}. \tag{10}$$

The scalar dissipation rate $\widetilde{\chi}_C$ is modeled using

$$\widetilde{\chi}_C = C\frac{\widetilde{c"^2}}{k/\varepsilon + \sqrt{\nu/\varepsilon}}. \tag{11}$$

The addition of the Kolmogorov time scale, $\sqrt{\nu/\varepsilon}$, is a common used treatment to prevent the time scale from becoming infinitely small, near wall, say. Under the assumption that chemical reactions produce maximum variance of the chemical progress, it can easily be shown that the variance equation can be replaced by the "compliment" of the variance, β, what is then solved by a transport equation. The variance is then defined by equation 12.

$$\widetilde{c"^2} = \widetilde{\alpha} - \widetilde{\beta} \tag{12}$$

with $\widetilde{\alpha} = \widetilde{c}(1-\widetilde{c})$ as the maximum variance. By this the spray variance source term is omitted. The mixture fraction and its variance are determined by equations (1) and (4) as described in section 2.1. The definition of the reactor size is then considered in the transport equation of the species, i.e. equation (13).

$$\frac{\partial}{\partial t}\overline{\rho}\widetilde{Y}_i + \nabla(\overline{\rho}\widetilde{\mathbf{u}}\widetilde{Y}_i) = -\triangle\mu_{eff}\widetilde{Y}_i + \kappa\dot{\omega}_i^R + \dot{S}_{i,evap}. \tag{13}$$

The source term of the chemistry, $\dot{\omega}_i = \kappa\dot{\omega}_i^R$, is controlled by the reactor size κ. It should be noted that the reactor has its own properties. The transport equation for the reactor species contains the chemistry source term (without the consideration of the reactor volume) and a mixing source term as shown in equation (14).

$$\frac{\partial}{\partial t}\overline{\rho}_R\widetilde{Y}_i^R + \nabla\cdot(\overline{\rho}_R\widetilde{\mathbf{u}}\widetilde{Y}_i^R) = -\triangle\mu_{eff}\widetilde{Y}_i^R + \frac{\overline{\rho}\widetilde{Y}_i - \overline{\rho}_R\widetilde{Y}_i^R}{\tau_{mix}} + \dot{\omega}_i^R. \tag{14}$$

The second term on the right hand side of this equation is the mixing source term, which defines the turbulence-driven mixing of the species inside the reactor with the "mean" species inside the computational cell. The transport equations for the reactor density and enthalpy are defined corresponding to equation (14). Here, the model defined in [3] is expanded upon by the definition of a reactor density, $\overline{\rho}_R$. The mixing term defines the interactions between the properties of the reactor and the mean properties of the cell. The turbulent mixing time, τ_{mix}, controls the mixing rate and is defined by

$$\tau_{mix} = C_{mix}\frac{\widetilde{k}}{\widetilde{\varepsilon}}. \tag{15}$$

The mixing constant C_{mix} is set to one in this study. However, in Figure 2 the results for different mixing constants (0.1, 1 and 5) at $p_{gas} = 42bar$, $T_{gas} = 1000K$ and 12% oxygen concentration are shown. The results of the predicted lift-off length with C_{mix} equal to 0.1 and 1 are very similar. With C_{mix}=5 the predicted lift-off length is shorter and the ignition slightly earlier. The smaller the mixing constant is as faster the reactor mixes with the mean properties. Following the results are

expected to be more similar to the well stirred reactor approach. This effect should be kept in mind while analyzing the results presented in this paper.

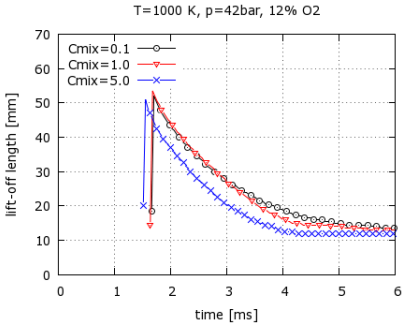

Figure 2. Lift-off length calculated with different mixing constants C_{mix} at $p_{gas} = 42bar$, $T_{gas} = 1000K$ and 12% oxygen concentration

The characteristic feature of the VRFM is its definition of a reactor volume. This makes it possible to consider the effects of chemistry and turbulence on the reaction rate simultaneously, without having to define turbulent and chemical time scales. The only quantity that is determined by a turbulent mixing time in this model is the mixing of the reactors properties with the mean properties of the cell. The distinction between the reactors properties and those of the cell as a whole reflects the fact that the reacting and non-reacting parts of a flow behave differently.

2.4 multiple RIF

The flamelet concept defines the chemical reaction zone as a thin laminar reaction layer (flamelet) within a turbulent flow field. The chemical reactions are not disturbed by turbulent eddies. In the representative interactive flamelet (RIF) model [4] the flamelet solution is coupled with the flow field. During non-premixed combustion the flamelet separates the oxidizer and the fuel, so the flamelet is bounded by the regions where Z=1 (fuel) and Z=0 (oxidizer). The flamelet's properties depend exclusively on the mixture fraction Z, the time t and the scalar dissipation rate χ. The advantage of this approach is that only the mixture fraction and its variance need to be solved in the 3-D domain of the flow-field. The chemistry is solved in the one-dimensional flamelet domain and depends only on the mixture fraction Z, meaning that it is decoupled from the flow field. The first-order flamelet equations for the species mass fraction and the temperature are given by equations (16) and (17) [23]:

$$\rho\frac{\widetilde{Y}_i}{\partial t} - \rho\frac{\chi}{2}\frac{\partial^2\widetilde{Y}_i}{\partial Z^2} = \dot{m}_i \tag{16}$$

$$\rho\frac{\widetilde{T}}{\partial t} - \rho\frac{\chi}{2}\frac{\partial^2\widetilde{T}}{\partial Z^2} - \rho\frac{\chi}{2c_p}\left[\sum_{i=1}^{n_s} c_{p_i}\frac{\partial\widetilde{Y}_i}{\partial Z} + \frac{\partial c_p}{\partial Z}\right]\frac{\partial\widetilde{T}}{\partial Z} = \frac{1}{c_p}\left(\frac{\partial p}{\partial t} - \sum_{i=1}^{n_s}\dot{m}_i h_i\right) \tag{17}$$

where h_i is the specific enthalpy of the specie and c_p the specific heat capacity. The flamelet equations are solved based on the averaged stoichiometric scalar dissipation rate χ_{st}, which is the only factor that couples the flow field and

the flamelet equations. A distribution of χ_{st} over the flamelet is defined. Because the scalar dissipation rate varies due to the inhomogeneity of the turbulent flow field and the mixture fraction distribution, Barths et. al [25] introduced the multiple RIF (mRIF) model. Several flamelets can be introduced by defining a tracer (marker particle) for each flamelet. The tracer then gives the probability of finding a flamelet l at a location $\overrightarrow{x}$ and time t, $\widetilde{I}_l(\overrightarrow{x},t)$. The flamelet solution is solely dependent on the mixture fraction. Once the flamelet solution has been obtained, its properties must be transformed back into the flow field domain. This is done by considering the mixture fraction and its variance. The transport equations for the mixture fraction, $\widetilde{Z}$, and its variance, $\widetilde{Z''^2}$, are those discussed previously, i.e. equations (1) and (4). The probability-density-function (pdf) of $\widetilde{Z}$ is assumed to be a β-pdf and the flamelet solution is integrated over the mixture fraction space. Together with the probability of finding a flamelet, the species mass fractions are defined based on multiple flamelet solutions using equation (18) [25].

$$\widetilde{Y}_i(\overrightarrow{x},t) = \sum_{l=1}^{n_f} \widetilde{I}_l(\overrightarrow{x},t) \int_0^1 \widetilde{P}(Z,\overrightarrow{x},t) Y_{i,l}(Z,t) dZ. \tag{18}$$

The surface averaged scalar dissipation rate under stoichiometric conditions for each flamelet is then calculated using the following expression:

$$\widehat{\chi_{st,l}} = \frac{\int_V \widetilde{I}_l(\overrightarrow{x}) \widetilde{\chi}_{st}^{3/2} \overline{\rho} \widetilde{P}(\widetilde{Z}_{st}) dV'}{\int_V \widetilde{I}_l(\overrightarrow{x}) \widetilde{\chi}_{st}^{1/2} \overline{\rho} \widetilde{P}(\widetilde{Z}_{st}) dV'}. \tag{19}$$

The subdivision of the CFD domain into different flamelet regions follows the approach of Vogel [26] and Lehtiniemi [27], which divides the domain into multiple flamelet regions based on the injected mass. More information about the implementation can also be found in [28]. Each flamelet "owns" a certain amount of the injected mass and different flamelets can overlap. Each new injected flamelet is initialized based on the previous one. Thirty flamelets were used in this work, each representing a specific portion of the injected mass. A new flamelet was thus introduced every 0.2 ms from the start of injection. **In Figure 3 the performance of the mRIF model is documented for different numbers of flamelets (1, 10, 20 and 30 flamelets) at a gas pressure of 42 bar, a gas temperature of 1000 K and an oxygen concentration of 21%. It is clear that the increase of the number of flamelets decreases the fluctuation of the predicted lift-off length. With just one flamelet the flame is attached to the nozzle. The difference between the results with 20 and 30 flamelets is very small and 30 flamelets were chosen to be accurate enough in this case. An increase of the number of flamelets also increases the computational time. The ignition delay is longer with 1 and 10 flamelets compared to 20 and 30 flamelets. One reason can be the higher dissipation rate for the injected flamelets that results in longer ignition delay. However, the results are dependent on the number of flamelets. This should be considered by analyzing the results.** D'Errico et al. [28] compared the performance of the WS model to the mRIF and introduced a new flamelet every 0.1 ms from the start of injection. Every new injected flamelet is cloned from the the previous one.

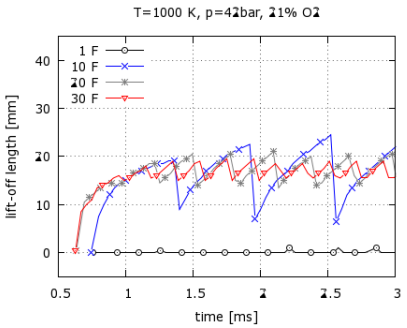

Figure 3. Lift-off length calculated with different number of flamelets at $p_{gas} = 42bar$, $T_{gas} = 1000K$ and 21% oxygen concentration

2.5 Differences Between the Models

The main differences between the different approaches for modeling turbulent non-premixed combustion are summarized in table 1.

Table 1. Comparison of combustion models

	mRIF	VRFM	WS
chemistry	$Y_i(Z,t)$ (decoupled from flow-field)	$Y_i(x,y,z,t)$	$Y_i(x,y,z,t)$
consideration of sub-grid turbulence-chemistry interaction	yes	yes	no

The VRFM and WS model both solve the chemistry for each cell in the CFD domain. Their computational costs are high and heavily dependent on the size of the chemical mechanism. The VRFM considers sub-grid turbulence-chemistry interactions by defining a reactor within each computational cell. The WS model does not consider any sub-grid scale effects. The mRIF model is based on a different approach to the modeling of turbulent combustion in which the chemistry is decoupled from the flow field and is simply solved in the 1-D domain of the mixture fraction. Consequently, the only variables that must be solved for in each CFD cell are the mixture fraction, its variance, and the flamelet tracers. The computational costs for this approach are considerably lower than those for the other two, and sub-grid scale effects are accounted for by considering the scalar dissipation rate. **The models have, mainly due to their approach of solving the chemistry, certain differences in computational time. An exact difference is difficult to define. The calculation time depends on the case and also for e.g. the number of flamelets in the mRIF model. However, computation times with the VRFM were discovered to be up to 7 times higher and the WS model up to 3.5 times higher compared to the mRIF model applied with 30 flamelets. These are gross numbers indicating the advantage of the mRIF model considering the computation time.**

2.6 Computational Configuration

All simulations were performed using the open source code OpenFOAM 2.0.x. The simulations are based on the Lib-ICE library, a set of applications and libraries for internal combustion engines developed by the ICE Group of Politecnico di Milano (e.g. [29], [30], [31]). The VRFM model was implemented in the same library to facilitate comparisons between the different combustion models using the same

spray library. The mRIF model has previously been tested and validated in [32] and [28]. Spray atomization and break-up were modeled using the Huh-Gosman model [33] and the Kelvin-Helmholtz break-up, respectively. The standard $k-\varepsilon$ model was used to model turbulence. The chosen chemistry for n-heptane oxidation is a reduced chemical mechanism based on the mechanism published in [34], that in turn was based on the detailed mechanism of Curran et al. [35]. This mechanism involves 35 species and 80 reactions. Because RANS simulations are symmetric, a 2D grid was used, simulating half of the spray cross-section area. The grid was a wedge mesh with a side length of 108 mm and a radius of 54 mm corresponding to the dimensions of the combustion vessel used in the experiments. The minimum cell size was 0.3 mm close to the nozzle. The use of a 2-D mesh reduced the number of cells to be considered and thus the computational time.

2.7 Experiments

The results of the simulations were compared to experimental data of the Engine Combustion Network. The measurements of an igniting n-heptane spray were done in a constant volume vessel chamber at Sandia National Laboratories and the results are available on the homepage of the network [15]. The conditions of the experiments are shown in table 2. The nozzle hole diameter is 100 μm and the

Table 2. Experimental conditions of spray H

Mole fraction O_2[%]	T_{gas} [K]	p_{gas} [bar]	p_{inj} [bar]
21	1000	42.1	1502
15	1000	42.5	1533
12	1000	42.7	1533
10	1000	42.8	1533
15	1000	87	1557
12	1000	87.4	1557
10	1000	87.6	1568

injection duration is 6 ms.

3. Results

3.1 Spray Validation

It is necessary to accurately describe the processes of spray break-up and mixing in order to reliably simulate ignition and combustion. A good description of the liquid and vapor penetration and the mixture fraction distribution within the spray will ensure that the spray is solved with reasonable accuracy. Figure 4 shows the results of a simulation of a non-burning spray generated under similar conditions to those described in section 2.7 with the same injection rate. Because the O_2-concentration is set to 0%, the spray cannot ignite. The gas pressure p_{gas} is 43.3 bar and the gas temperature T_{gas} is 1000K.

The predicted liquid and vapor penetration lengths agree well with the experimental measurements. The liquid penetration is defined as the distance between the injection cell and the cell for which 95% of the total liquid is in cells closer to the injector tip. The vapor penetration is defined as the distance between the injection cell and the cell furthest downstream of the spray with a vapor concentration of at

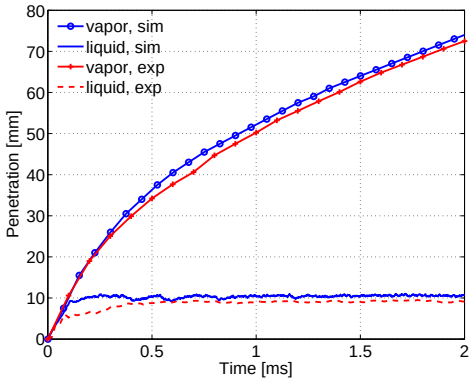

Figure 4. Vapor and liquid penetration

least approximately 1 %. The mixture fraction was also predicted reasonably well, as shown in Figure 5. The k-ε turbulence model was tuned **under the conditions presented here** (C_1=1.55, σ_ε=1.4) to achieve a reasonable agreement between the experimental and simulated data for both of the penetration curves (cf. Figure 4) and the mixture fraction (Figure 5).

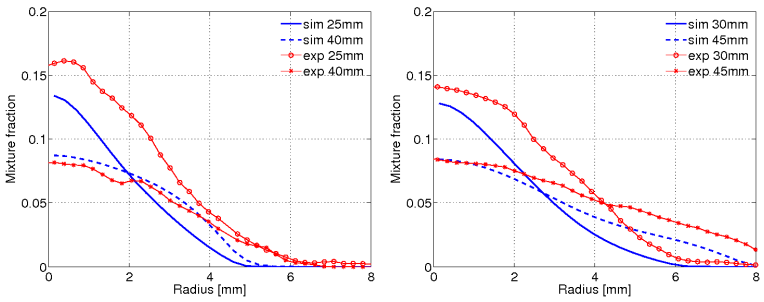

(a) 0.68 ms ASOI (b) 1.13 ms ASOI

Figure 5. Radial mixture fraction distribution at 0.68 ms and 1.13 ms ASOI at different axial distance from the injector (25 & 40 mm at 0.068ms ASOI, 30 & 45 mm at 1.13ms ASOI)

3.2 Ignition delay

Figures 6 (a) and (b) show the ignition delay predicted with the VRFM, the WS model and the mRIF model compared to the experimental results at gas pressures of 42 bar and 87 bar (14.8 and 30 kg/m^3). The ignition delay is defined as the amount of time between the start of injection and the occurrence of a sharp and pronounced temperature increase that happens within 0.1 ms of the start of injection and is accompanied by a sudden increase in H_2O_2 **and OH** production. **With this definition the ignition delay is accurate within a tenth of a second.** In all cases involving high gas pressure or low gas pressure with a high O_2 concentration, the temperature increases by several hundred Kelvin within this 0.1 ms window **and the definition of the ignition delay is straightforward**. At low gas pressure and low oxygen concentration, the temperature rise is less steep **what makes the definition more difficult**. However, as mentioned in [36] "it has been found that ignition-delay results are relatively insensitive to the exact definition that is used". At high gas pressure (Figure 6 (a)), the ignition delay was captured well by all three models. The ignition delay increases as the mole fraction of O_2 in the gas phase decreases, because the reaction rate decreases. As shown in Figure 6 (b), the predicted ignition delay at the lower gas pressure was longer than the ex-

perimental value, with the difference being most pronounced at the lowest oxygen concentration. It is difficult to define the start of ignition under such conditions, which may be part of the reason for the relatively large difference. However, there was no appreciable or systematic difference between the tested models in terms of the gap between the predicted and measured ignition delays under these conditions. **One reason for the longer ignition delay under these conditions could therefore be the chemical mechanism used in the simulations. Another reason could be attributed to the combustion models.**

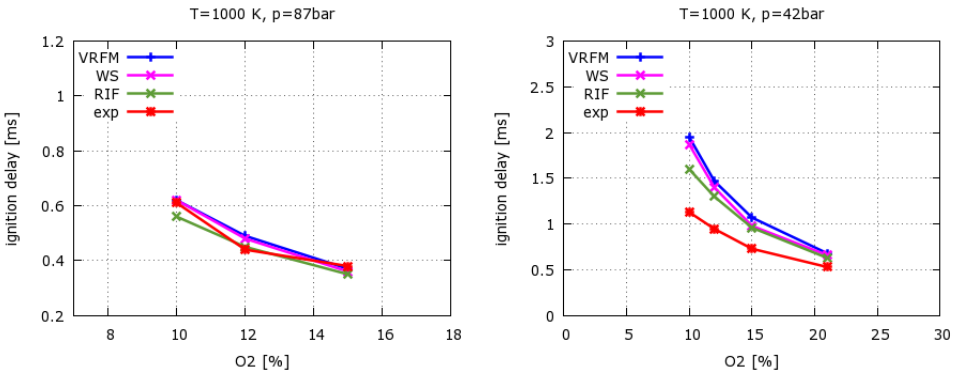

(a) $p_{gas} = 87bar$ (b) $p_{gas} = 42bar$

Figure 6. Ignition delay

3.3 Lift-off length

Figures 7 (a) and (b) compare the lift-off lengths predicted in the simulations to the experimental data. The lift-off length is defined as the shortest distance between the nozzle orifice and the region where the OH concentration is 2% of its maximum value, in keeping with the ECN's recommendations. The lift-off length was underpredicted in all of the simulations. At a gas pressure of 87 bar (Figure 7 (a)) the VRFM and the WS model gave better results than the mRIF model, but all models predict the lift-off length reasonably well. The trend of the lift-off length to increase at lower O_2-concentrations is captured by all of the models. It should be noted that it is somewhat more difficult to define the lift-off length when using the mRIF model than with the other models. This is because each flamelet has its own ignition delay that depends on its scalar dissipation rate. After ignition, the flamelet solution depends on the mixture fraction and with just one flamelet the flame lift-off would be very short because the mixture fraction is stoichiometric also close to the nozzle. With several flamelets, each of which must ignite separately, the lift-off length must be determined by considering the autoignition of each flamelet and the scalar dissipation rate. Because there are multiple igniting flamelets, the lift-off position fluctuates, what is defined as uncertainties. As the number of flamelets considered in the simulation increases, these uncertainties become less pronounced. Furthermore new injected flamelets are cloned by the previous one, what reduces the ignition delay of the single flamelets. The uncertainties in the simulations conducted within this study are shown in Figures 7 (a) and (b). In the low gas pressure cases with 21 and 15 % O_2, the mRIF model was able to predict the lift-off length correctly. Both the VRFM and the WS model underpredict the lift-off length, but the VRFM gave slightly better results than the WS model. The longer lift-off lengths predicted using the VRFM

and the mRIF model are due to their incorporation of sub grid scale effects. Conversely, the WS model assumes that each computational cell is well-mixed when in reality there may be significant intra-cell variation in the mixture fraction due to evaporation. It would therefore predict that reactions would occur in some cells where adequate mixing has not occurred on the sub grid scale. This is the case close to the nozzle, where the spray is evaporating and the vapor must mix with the air before it can ignite. Therefore, the WS model allows ignition and reactions to occur in cells that are relatively close to the nozzle, reducing the calculated lift-off length. This does not occur under the mRIF model and VRFM, which do consider sub-grid scale effects and only allow reactions to occur if mixing has occured. However, the difference between the VRFM and the WS model is small **, what indicates a minor influence of the reactor definition in the VRFM. One reason can be small variances of chemical progress and mixture fraction.** The stabilization process of the VRFM and WS model is controlled by the flame front that propagates upstream and the counter flow of the spray that moves downstream. These two effects are balanced at the flame stabilization point. Both models consider local conditions in each cell for the chemistry solution. The lift-off length with the mRIF model instead is controlled by the auto-ignition of the different flamelets. However, the mRIF model gives the best results in such cases. Different results were obtained for cases with lower O_2 concentrations and

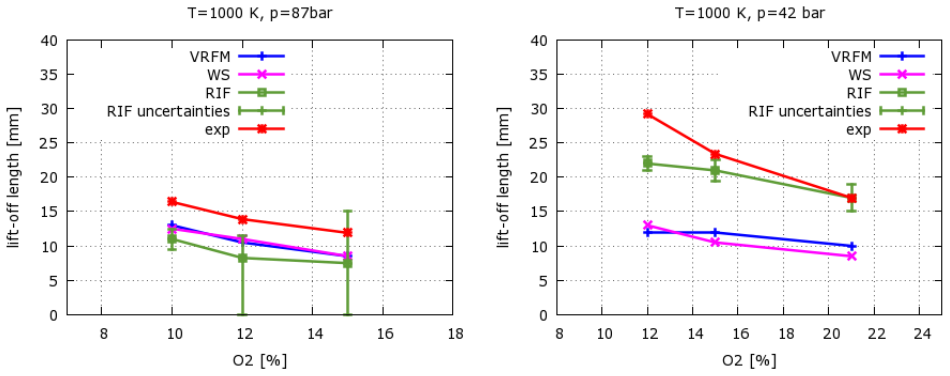

(a) $p_{gas} = 87bar$ (b) $p_{gas} = 42bar$

Figure 7. Lift-off length

low gas pressure (p_{gas} = 42 bar, O_2=10-12%). The transient lift-off length is shown in Figure 8 (a) and (b). The change in the calculated lift-off length over time is interesting because it reflects the development of the flame along the spray axis. Under the VRFM and the WS model, the flame ignites closer to the spray tip and then propagates upstream along the spray. This is a well known physical progress and was also shown experimentally by e.g. [37] and was already predicted by [5]. In case of fast ignition this effect is not as pronounced compared to cases with longer ignition delay, because the spray did not yet penetrate further. Under the mRIF model the flame lift-off length increases slowly and then it stabilizes. The mRIF model is not able to predict a certain ignition position, because the flamelets ignite each on their own. Therefore it is also not possible to reproduce the flame propagation along the stoichiometric mixture as it is seen with the VRFM and WS model. However, the lift-off lengths calculated using the WS model for cases with O_2 concentrations of 10-12 % at later times after start of injection (ASOI) are larger than those predicted by the VRFM. This was unexpected given the explanation invoked above to explain the shorter lift-off lengths predicted by the WS model in cases with high gas pressure and/or higher O_2 concentrations. However, similar behavior

has previously been reported by Pei et. al [38] who simulated the n-heptane spray cases from the ECN and compared the performance of the WS model to that of an alternative PDF model: they found that at low oxygen concentrations, the WS model predicted a much longer lift-off length. Bhattacharjee [36] also compared the PDF method to a WS model and observed a similar effect, although it was less pronounced than in our study or that presented by Pei et al. [38]. There are sev-

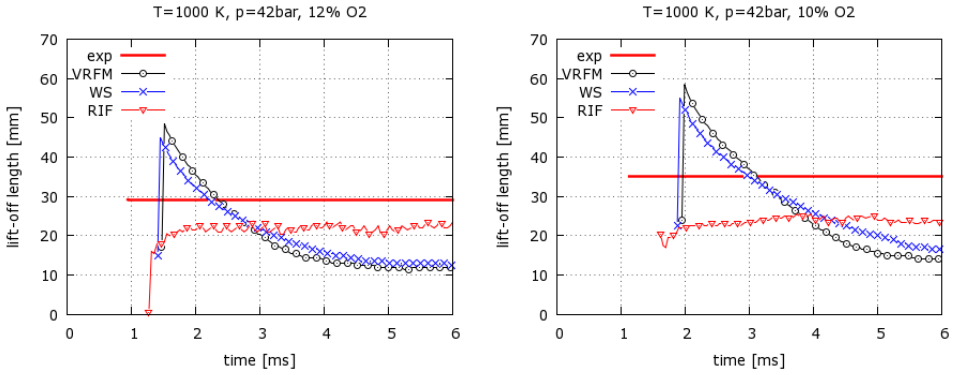

(a) $p_{gas} = 42bar, 12\%O2$ (b) $p_{gas} = 42bar, 10\%O2$

Figure 8. Lift-off length

eral competing processes that may contribute to this finding. First, the WS model assumes each cell to be well-mixed even if there is strong intra-cellular variation in the mixture fraction. Consequently, a cell may be assumed to be sufficiently mixed to enable reactions to occur even when this is not realistic. In such cases, the mixture would be predicted to ignite sooner than it should. However, this is counterbalanced by the fact that the mean temperature in the cell is lower than the reactor temperature in the VRFM, and lower temperatures reduce the rate of reaction. This effect becomes more pronounced in low pressure situations, because the lower density causes a stronger cooling of the gas phase as the liquid phase evaporates. Because the cooling depends only on the gas density and is independent of the oxygen concentration, this effect is considered to be identical for all cases with the same gas pressure and temperature. Finally, if the chemistry is slow, excessively rapid mixing of the igniting mixture with fresh air will disturb the progress of the reactions and slow down ignition. One explanation for the shorter lift-off length predicted with the VRFM could be the definition of the reactor. The reactor size is defined based on variances in mixture fraction and chemical progress. A mixing term in the transport equations of the reactor properties considers the mixing of the reactor properties with the mean. The source of fuel species for the reactor is hence just the mixing of the reactor species with the mean species. Here the mixture fraction within the reactor is smaller compared to the mean mixture fraction ($Z_R < Z$). With a smaller mixture fraction the cooling of the reactor is also less than the one of the mean cell. Additionally, the mixing of the reactor properties with fresh gas is depending on the mixing term. At these conditions the dwell time of the reacting species in the reactor (even if it is a small reactor volume due to the strong variances in mixture fraction) might be long enough to ignite the mixture while the mean cell (where the temperature is lower and the mixing faster) is not igniting. **The results of the sensitivity of the choice of the mixing constant C_{mix} in the VRFM, documented in section 2.3, underline these explanations. A slower mixing of the reactor properties with the mean properties results in shorter lift-off length.** However, some more investigations are needed to proof it. Figure 9 shows the changes in the temperature inside

a homogeneous reactor during ignition under three different initial conditions. As can be seen, the first stage ignition process takes much longer with an initial O_2 concentration of 10% in the gas phase and a gas pressure of 42 bar than in the case with 21% O_2 and $p_{gas} = 42$ bar. The cool flame develops for 2 ms in the case with 10% O_2 and the second stage ignition takes place after 2.2 ms. Conversely, with 21% O_2 the mixture ignites within 0.65 ms. The maximum temperature after ignition is several hundred Kelvin lower in the case with 10% O_2 than in that with 21% O_2. This is because the low O_2 concentration in the former case makes the chemistry much slower. The influence of the gas density can be seen by comparing the temperature development at gas pressures of 42 bar and 87 bar. The lower gas pressure and density greatly reduces the rate of first stage ignition because with lower density the number of molecule collisions decreases and hence the reaction rate. However, the choice of the chemical mechanism also has a profound influence

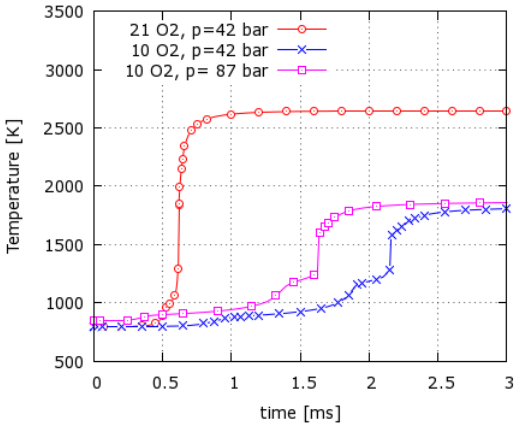

Figure 9. Comparison of temperature development during ignition with 21% and 10% O_2 in the gas phase

on the results obtained as was demonstrated in [39].

3.4 Temperature Development

Figures 10-12 show scatter plots of the temperature T depending on the mixture fraction Z at different ambient conditions and times ASOI. Figure 10 shows the predicted temperatures at 87 bar (high pressure) and 15 % O_2. On the lean side the temperatures are similar with all models. The WS model predicts the highest temperatures at 0.5 ms ASOI (Figure 10 (a)). Higher temperatures with the WS model are expected due to the fact that the chemical source term is not controlled by any subgrid scale effects and the whole cell reacts. In the VRFM and mRIF model not all vapor fuel is reacting immediately. At later times ASOI (Figures 10 (b)-(c)) the difference between the VRFM and WS model is small. The mRIF model shows reactions in the rich region because the flamelets close to the nozzle ignite very fast. In Figures 11 (a)-(c) and 12 (a)-(c) the VRFM and WS model predict significant higher temperatures in the rich area compared to the mRIF model. At these conditions the lift-off length was predicted significant shorter with the VRFM and WS model compared to the mRIF model. Therefore one explanation for the underprediction of the lift-off length of the VRFM and WS model can be the fact that they allow reactions to occur in much richer regions (fuel rich zone in the spray core) compared to the mRIF model. The mRIF model does not react in richer regions due to the fact that the flamelets close to the nozzle, where the mixture fraction is largest, are the last injected ones and not ignited yet. Another

interesting result is the difference between the VRFM and WS model. The temperature predicted with the WS model is in general higher at mixture fractions where also the VRFM reacts. This is, as explained before, expected due to the fact that the chemical source term is controlled in the VRFM. Significant differences are shown in Figure 12 (c) at later times ASOI. At 42 bar gas pressure and 10% oxygen concentration (Figure 12 (c)) the VRFM reacts at larger mixture fractions compared to the WS model. At these conditions the VRFM predicts a shorter lift-off length. What is also interesting is how the different temperatures are distributed at certain mixture fractions. At 42 bar gas pressure and 10% oxygen concentration (Figure 12) the temperature is quite distributed between the maximum and minimal temperature at a certain mixture fraction where reactions occur. At 87 bar and gas pressure and 15% oxygen concentration (Figure 10) the temperatures are either high (burning) or low (not burning) and less distributed. That indicates again that at 42 bar gas pressure and 10% oxygen concentration the chemistry is slow enough to be disturbed by the mixing with fresh gas. The combustion is not just mixing controlled. This underlines the explanation of the cooling effect and slower chemistry on the reaction rate that was already discussed in section 3.3, what results in a longer lift-off length with the WS model compared to the VRFM. The reactor in the VRFM creates conditions ($Z_R < Z$ with $T_R > T$) that allow reactions and has an opposite effect compared to the cases with fast chemistry.

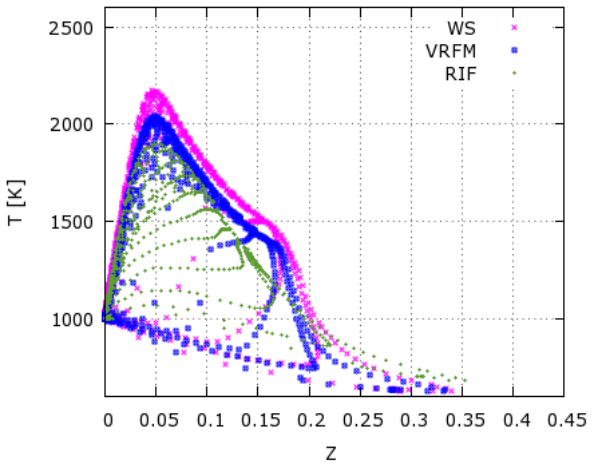

(a) 0.5 ms ASOI

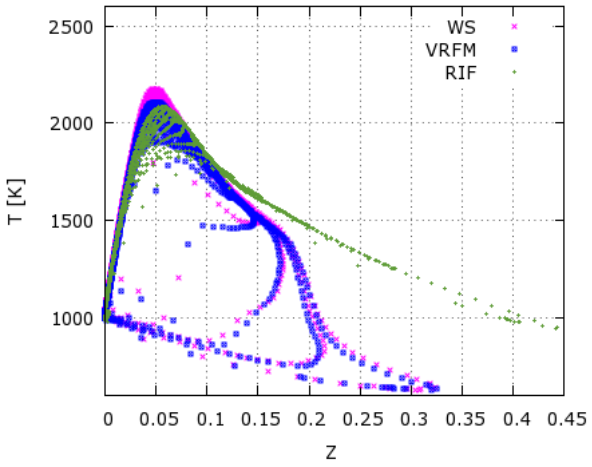

(b) 1 ms ASOI

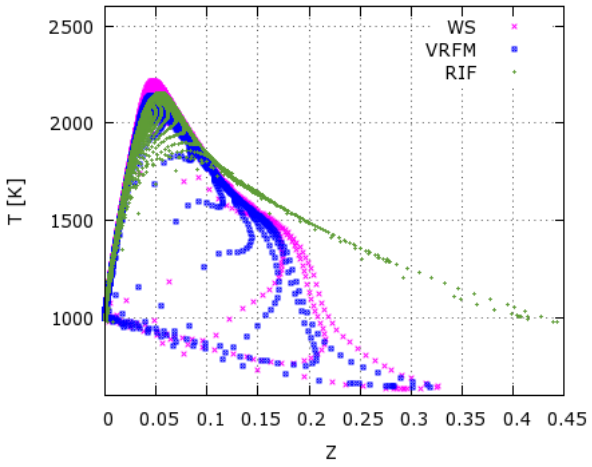

(c) 2 ms ASOI

Figure 10. Predicted temperature depending on the mixture fraction Z at $T_{gas} = 1000K, p_{gas} = 87bar, 15\%O_2$

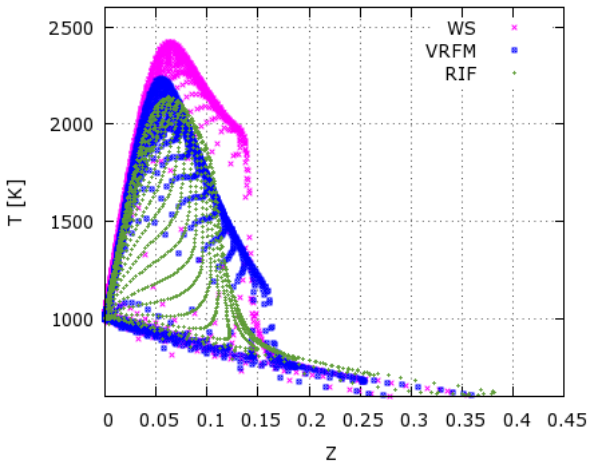

(a) 0.8 ms ASOI

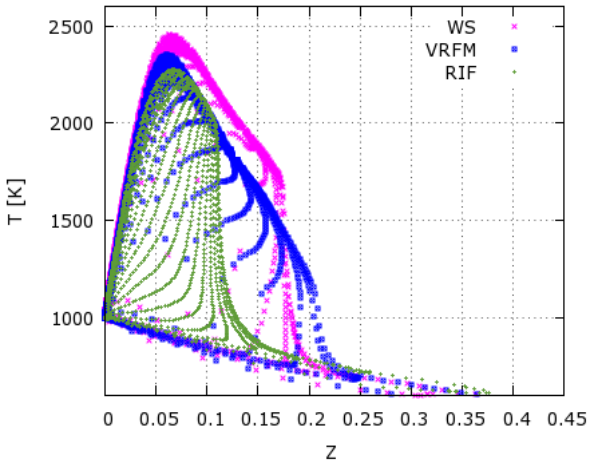

(b) 1 ms ASOI

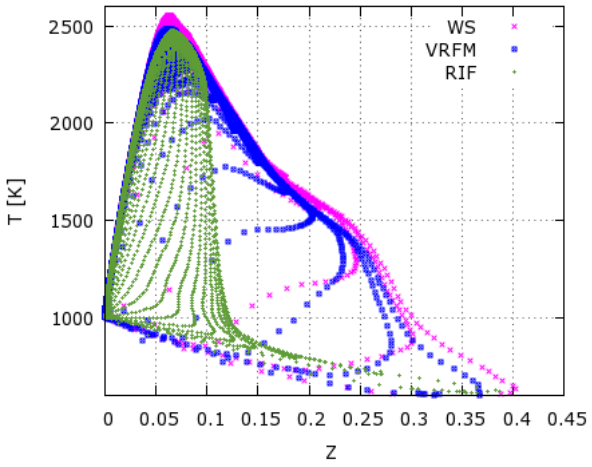

(c) 3 ms ASOI

Figure 11. Predicted temperature depending on the mixture fraction Z at $T_{gas} = 1000K, p_{gas} = 42bar, 21\%O_2$

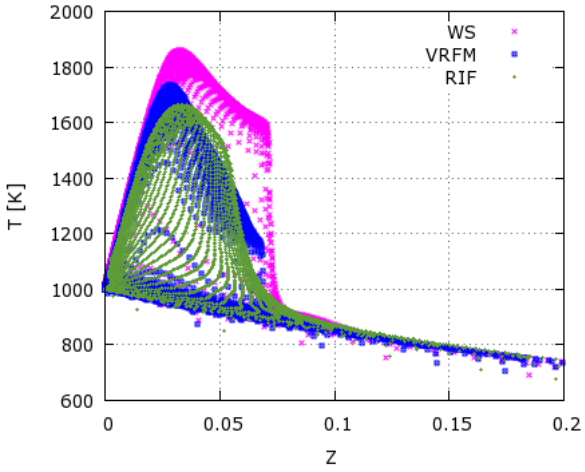

(a) 2.3 ms ASOI

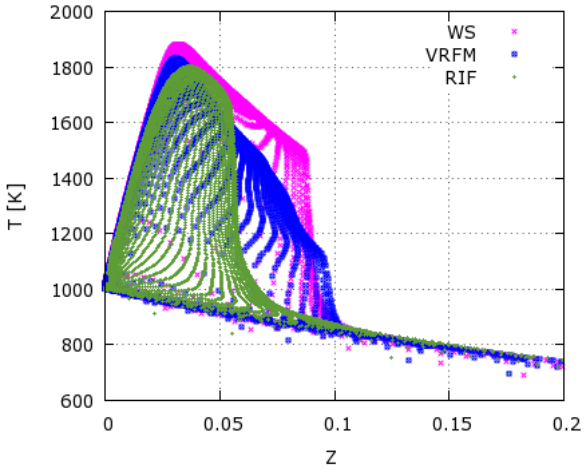

(b) 3.5 ms ASOI

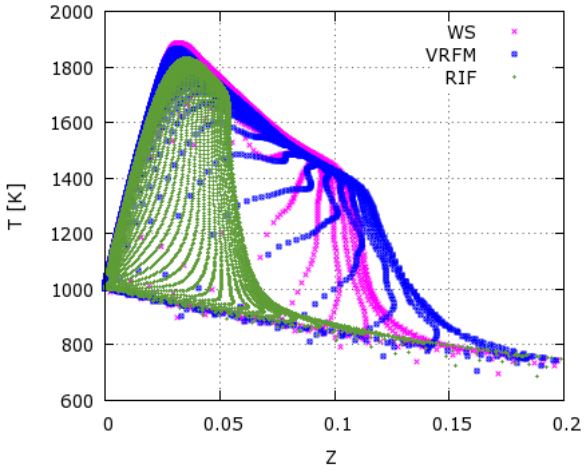

(c) 4.8 ms ASOI

Figure 12. Predicted temperature depending on the mixture fraction Z at $T_{gas} = 1000K, p_{gas} = 42bar, 10\%O_2$

3.5 Flame structure in physical space

Figures 13-14 show the predicted temperature and OH fields at different times ASOI at 42 bar gas pressure with an oxygen concentration of 10%. At these conditions the difference between the models is very clear. There are some notable differences between the flame structures predicted by the mRIF model and those obtained with the VRFM and WS model. In particular, the WS model and VRFM yield a well-defined flame stabilization point that is not observed with the mRIF model. Instead, the mRIF model flame is more diffuse. The highest predicted temperature and OH concentration are obtained with the WS model, followed by the VRFM. This result was expected because of the limited chemical source term in the VRFM. The VRFM and the WS model both predict that ignition occurs in the spray tip and that a triple flame then moves upstream after ignition. This behavior is not seen with the mRIF model. The mRIF model is not able to predict a local ignition position.

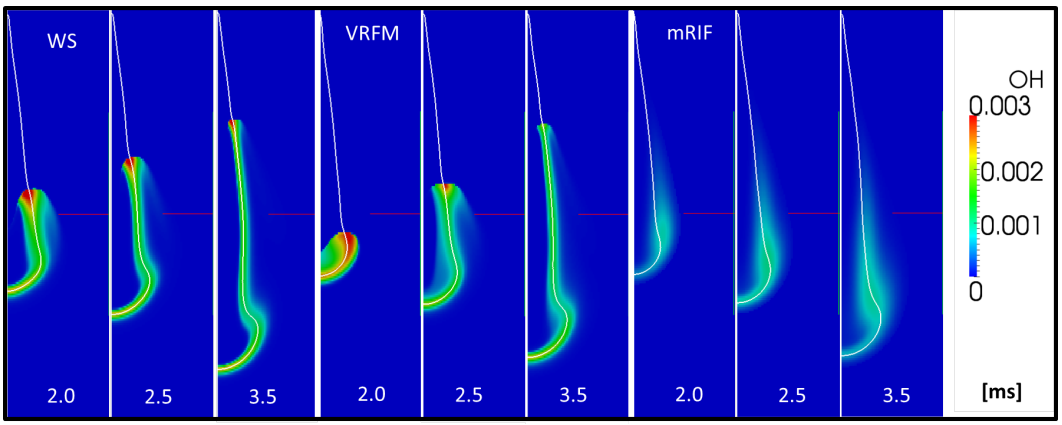

Figure 13. Predicted OH field at different time ASOI, $T_{gas} = 1000K, p_{gas} = 42bar, 10\%O_2$

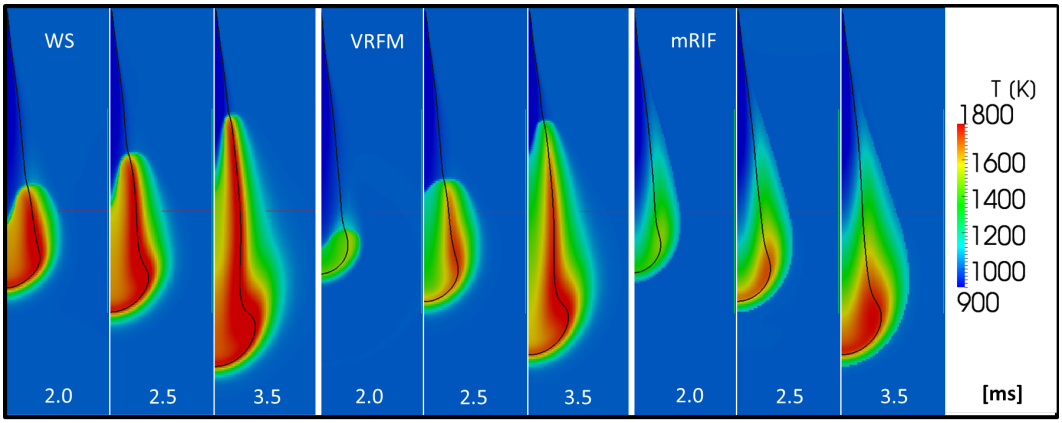

Figure 14. Predicted temperature field at different time ASOI, $T_{gas} = 1000K, p_{gas} = 42bar, 10\%O_2$

4. Conclusion

The processes that stabilize Diesel flames are complex and not well understood at present. This work compared the performance of the multiple representative interactive flamelet (mRIF) model, the Volume Reactor Fraction Model (VRFM) and the well-stirred reactor (WS) model, all of which were implemented in the same software package. The simulated ignition delay and lift-off length of an n-heptane flame were compared to experimental data published by the Engine Combustion Network (ECN). All models were able to correctly predict the experimental trends in ignition delay and lift-off length at different gas pressures and oxygen concentrations. The calculated ignition delays did not differ greatly between the models, but were strongly overpredicted in all cases at low gas pressure (p_{gas} = 42 bar) compared to the experimental values.

The quality of the predicted lift-off lengths depended on the simulated ambient conditions. The VRFM gave the best results at high gas pressure (p_{gas} = 87 bar), followed by the WS model, while the mRIF model afforded the shortest predicted lift-off lengths. At low gas pressure (p_{gas} = 42 bar) and oxygen concentrations of 21% or 15% O_2, the mRIF model offered the best performance and accurately predicted the lift-off length. The VRFM and WS model both underpredicted the lift-off length, but the VRFM's predictions were closer to the experimental values. At the low gas pressure (p_{gas} = 42 bar) and low oxygen concentrations (10-12%), the predicted lift-off lengths were unsteady and those obtained with the WS model were larger than those with the VRFM.

The results of the simulations imply that the physical processes that govern flame stabilization vary with the concentration of oxygen in the gas phase. The gas phase dynamics, especially in the region close to the nozzle, were assumed to be identical in each case because the same mass rate profile was applied during injection in all of the simulations. In addition, the cooling of the gas phase depends only on the gas density and does not change with the oxygen concentration. The shorter predicted lift-off length with the VRFM model at low pressures and oxygen concentration indicates that the reactor in the VRFM creates an igniting surrounding ($Z_R < Z$ with $T_R > T$) while the mean properties in the WS model are not igniting. A more detailed investigation will be required to properly test this assumption. However, it is clear that the behaviors of the VRFM and the WS model at the low gas pressure (p_{gas}=42 bar) depend strongly on the oxygen concentration. **The chemistry is significant slower at these conditions and the assumption of fast chemistry is maybe not correct for these conditions.** Similar findings have been reported previously in studies that compared the WS model to the PDF model ([38], [36]). The flame development and flame structure are similar with the VRFM and WS model. Both predict the ignition close to the spray tip and a triple flame is propagating upstream until the flame stabilizes. The mRIF model is not able to capture a local ignition position, because each flamelet ignites on his own. Therefore it is also not possible to reproduce flame propagation with the mRIF model. The lift-off length is controlled by auto-ignition of the different flamelets.

It should be emphasized that the primary aim of this work was to compare the different models rather than to identify the best model for predicting lift-off lengths. Moreover, it is important to note that the results obtained in simulations are strongly dependent on the chemical mechanism that is used, as shown by [39].

It is therefore possible that very different results may have been obtained in this work if a different mechanism had been used. However, given that the simulations reported herein were conducted using identical computational set-ups and models for all processes other than the turbulence-chemistry interaction, the results obtained should provide a good comparison of the tested turbulence-chemistry models.

This work points out the need to define regime independent models that are able to capture both high pressure and temperature conditions with fast chemistry but also low pressure and temperature cases with significant slower chemistry. The assumption of fast chemistry, as it is usually done in combustion models for non-premixed combustion, is not true for all conditions presented in this paper. The coupling of non-premixed turbulent combustion models with an approach for premixed turbulent combustion is a next step to improve the prediction of fuel spray combustion.

References

[1] N. Peters, *Laminar Diffusion Flamelet Models in Non-Premixed Turbulent Combustion*, Prog. Energy Combustion Science 10 (1984), pp. 319–339.

[2] D. Spalding, *Mixing and Chemical Reaction in Steady Confined Turbulent Flames*, 13th Symposium on Combustion, The Combustion Institute (1971), pp. 649–657.

[3] A. Kösters, V. Golovitchev, and A. Karlsson, *A Numerical Study of the Effect of EGR on Flame Lift-off in N-Heptane Sprays Using a Novel PaSR Model Implemented in OpenFOAM*, SAE Int. J. Fuel and Lubricants 5(2) (2012), pp. 604–610.

[4] H. Pitsch, *Modellierung der Zündung und Schadstoffbildung bei der dieselmotorischen Verbrennung mit Hilfe eines interaktiven Flamelet-Modells*, Dissertation, RWTH Aachen, 1998.

[5] J. Chomiak and A. Karlsson, *Flame Lift-Off in Diesel Sprays*, 26th Symposium (International) on Combustion, The Combustion Institute (1996), pp. 2557–2564.

[6] B. Magnussen, *On the Structure of Turbulence and Generalized Eddy Dissipation Concept for Chemical Reaction in Turbulent Flow*, 19th AIAA Sc. Meeting (1981).

[7] B. Magnussen and B. Hjertager, *On Mathematical Modeling of Turbulent Combustion with Special Emphasis on Soot Formation and Combustion*, 16th Symposium (International) on Combustion, The Combustion Institute (1976), p. 719.

[8] J.A.J. Karlsson, *Modeling Auto-Ignition, Flame Propagation and Combustion in Non-Stationary Turbulent Sprays*, Ph.D. thesis, Chalmers University of Technology, 1995.

[9] P.A.N. Nordin, *Complex Chemistry Modeling of Diesel Spray Combustion*, Ph.D. thesis, Chalmers University of Technology, 2001.

[10] F.P. Kärrholm, *Numerical Modelling of Diesel Spray Injection, Turbulence Interaction and Combustion*, Ph.D. thesis, Chalmers University of Technology, 2008.

[11] S. Hong, M. Wooldridge, and D. Assanis, *Modeling of Chemical and Mixing Effects on Methane* , Proc. Combustion Inst, The Combustion Institute 29(1) (2002), pp. 711–716.

[12] S. Kokjohn and R. Reitz, *Investigations of the Roles of Flame Propagation, Turbulent Mixing, and Volumetric Heat Release in Conventional and Low Temperature Diesel Combustion*, ASME J. Eng. Gas Turbines Power 133 (2011).

[13] S. Singh, R. Reitz, and M. Musculus, *Comparison of the Characteristic Time (CTC), Representative Interactive Flamelet (RIF), and Direct Integration with Detailed Chemistry Combustion Models against Optical Diagnostic Data for Multi-Mode Combustion in a Heavy-Duty DI Diesel Engine*, SAE technical paper 2006-01-0055 (2006).

[14] S.C. Kong and R. Reitz, *Multidimensional Modeling of Diesel Ignition and Combustion Using Multistep Kinetics Model*, Int. Journal of Engineering for Gas Turbines and Power 115, pp. 781–789.

[15] Engine Combustion Network, http://www.sandia.gov/ecn; .

[16] Y. Pei, E. Hawkes, and S. Kook, *A Comprehensive Study of Effects of Mixing and Chemical Kinetic Models on Predictions of n-heptane Jet Ignitions with the PDF Method.*, Flow, Turbulence and Combustion 91(2) (2013), pp. 249–280.

[17] J. Dec, *A Conceptual Model of DI Diesel Combustion Based on Laser-Sheet Imaging*, SAE technical paper 970873 (1997).

[18] J. Dec, zur Loye, and D. Siebers, *Soot Distribution in a D.I. Diesel Engine Using 2-D Laser-Induced Incandescence Imaging*, SAE technical paper 910224 (1991).

[19] Y.H. Won, T. Kamimoto, H. Kobayashi, and H. Kosaka, *2-D Soot Visualization in Unsteady Spray Flame by means of Laser Sheet Scattering Technique*, SAE technical paper 910223 (1991).

[20] R. Ragucci, A. Cavaliere, and A. D'Alessio, *Laser Assisted Diagnostics for Characterization of Condensed Phases During Diesel Combustion Processes*, Proc. of the International Symposium on Diagnostics and Modeling of Combustion in Internal Combustion Engines, COMODIA 90 (1990), pp. 371–376.

[21] L. Pickett, D. Siebers, and C. Idicheria, *Relationship Between Ignition Processes and the Lift-Off Length of Diesel Fuel Jets*, SAE technical paper 2005-01-3843 (2005).

[22] J. Réveillon and L. Vervisch, *Spray vaporization in non-premixed turbulent combustion modeling: a single droplet model*, Combustion and flame 121 (2000), pp. 75–90.

[23] C. Hasse, *A two-dimensional flamelet model for multiple injections in diesel engines*, Dissertation, RWTH Aachen, 2004.

[24] S. Burke and T. Schumann, *Diffusion Flames*, Proceedings of the Combustion Institute 1 (1928), pp. 2–11.

[25] H. Barths, C. Hasse, G. Bikas, and N. Peters, *Simulation of Combustion in Direct Injection Diesel Engines Using an Eulerian Particle Flamelet Model*, Proceedings of the Combustion Institute 28 (2000), pp. 1161–1168.

[26] S. Vogel, *Coupling of a Level-Set Model for Premixed Combustion with a Diffusion Flamelet Model*, RWTH Aachen, 2008.

[27] H. Lehtiniemi, Y. Zhang, R. Rawat, and F. Mauss, *Efficient 3-D CFD Combustion Modeling with Transient Flamelet Models*, SAE technical paper 2008-01-0957 (2008).

[28] G. DErrico, T. Lucchini, F. Contino, M. Jangi, and X.S. Bai, *Comparison of well-mixed and multiple representative interactive flamelet approaches for diesel spray combustion modelling*, Combustion Theory and Modelling 18(1) (2014), pp. 65–88.

[29] T. Lucchini, G. D'Errico, D. Ettorre, and G. Ferrari, *Numerical Investigation of Non-Reacting and Reacting Diesel Sprays in Constant-Volume Vessels*, SAE Int. J. Fuel and Lubricants 2(1) (2009), pp. 966–975.

[30] A. Montanara, L. Allocca, D. Ettorre, F. Brusiani, and G. Cazzoli, *Experimental Characterization of High-Pressure Impinging Sprays for CFD Modeling of GDI Engines*, SAE Int. J. Engines 4(1) (2011), pp. 747–763.

[31] F. Contino, T. Lucchini, G. D'Errico, C. Duynslaegher, V. Dias, and H. Jeanmart, *Simulations of Advanced Combustion Modes Using Detailed Chemistry Combined with Tabulation and Mechanism*

Reduction Techniques, SAE Int. J. Engines 5 (2012), pp. 185–196.

[32] P. Colombi, *Development and Validation of a CFD Model for Combustion Simulations in Direct Injection Diesel Engines Based on Detailed Chemistry and the Unsteady Diffusion Flamelet Assumption*, Master Thesis, Politecnico di Milano, 2012.

[33] K. Huh and A. Gosman, *A Phenomenological Model of Diesel Spray Atomization*, Proc. Int. Conf. of Multiphase Flow (1991).

[34] T. Rente, V. Golovitchev, and I. Denbratt, *Effect of Injection Parameters on Auto-Ignition and Soot Formation in Diesel Sprays*, SAE technical paper 2001-01-3687 (2001).

[35] H. Curran, P. Gaffuri, and C. Pitz P. Westbrook, *A Comprehensive Modeling Study of iso-Octane Oxidation*, Combustion Flame 114 (1998), pp. 149–177.

[36] S. Bhattacharjee and D. Haworth, *Simulations of transient n-heptane and n-dodecane spray flames under engine-relevant conditions using transported PDF method*, Combustion and Flame 160 (2013), pp. 2083–2102.

[37] R. Ochoterena, *Optical Diagnostics of Soot in Combusting Sprays*, Chalmers University of Technology, 2009.

[38] Y. Pei, E. Hawkes, and S. Kook, *Transported probability density function modelling of the vapour phase of an n-heptane jet at diesel engine conditions*, Proc. Combustion Inst., The Combustion Institute 34(2) (2013), pp. 3039–3047.

[39] M. Bolla, T. Gudmundsson, Y. Wright, and K. Boulouchos, *Simulations of Diesel Sprays Using the Conditional Moment Closure Model*, SAE Int. J. Engines 6(2) (2013).